Electronic Supplementary Material (ESI) for Faraday Discussions.

Supporting Information

Substituent Effects on Through-Space Intervalence Charge Transfer in Cofacial Metal-Organic Frameworks

Patrick W. Doheny,[a] Carol Hua,[a,b] Bun Chan,[c] Floriana Tuna,[d] David Collison,[d] Cameron J. Kepert[a]* and Deanna M. D'Alessandro [a]*

[a] School of Chemistry, The University of Sydney, New South Wales, 2006 Australia

[b] School of Chemistry, The University of Melbourne, Victoria, 3010 Australia

[c] Graduate School of Engineering, Nagasaki University, Nagasaki 852-8521, Japan

[d] Department of Chemistry and Photon Science Institute, The University of Manchester, Manchester M13 9PL, United Kingdom.

*Corresponding authors' phone: +61 2 93513777; email: deanna.dalessandro@sydney.edu.au; cameron.kepert@sydney.edu.au

Additional Instrumental Details

Thermal Gravimetric Analysis (TGA). TGA analysis was performed using a TA Instruments Discovery Thermogravimetric Analyser from 25-600 °C at 2 °C min^{-1} under a flow of nitrogen gas (0.1 L min^{-1}).

Inductively Coupled Plasma Mass Spectrometry (ICP-MS). ICP-MS measurements were performed using a Perkin Elmer Nexion 300X. Samples were open digested in concentrated HNO_3 overnight at room temperature before dilution with milliQ water to a 1 ppm - 1 ppb concentration range. Calibration curves were constructed with Cu, Cr, Fe, Co as a mixed standard using a Hamilton autodiluter. Samples and standards were spiked with a standard mix of Sc, Rh and Ir as internal standards. All elements were measured in standard and KED mode (helium gas 5 L min^{-1}).

Additional Crystallographic Details

Crystallography of BPPFTzTz. A single, yellow plate crystal of the BPPFTzTz ligand was mounted using a thin film of Paratone *N* oil on a diffractometer employing a Dectris EIGER X 16M detector and Silicon Double Crystal monochromated synchrotron radiation in a stream of nitrogen gas at 100(2) K at the MX2 beamline of the Australian synchrotron.[1] The structure was solved by intrinsic phasing in the monoclinic $P2_1/c$ (#14) space group using the SHELXT[2] program with further refinements and computations carried out using SHELXL-2018/3[3] within the ShelXle graphical user interface.[4] The non-hydrogen atoms in the asymmetric unit were modelled with anisotropic displacement parameters and a riding model with group displacement parameters for the hydrogen atoms. Despite the use of high intensity synchrotron radiation, the crystals exhibited poor diffraction quality with a maximum resolution of 1.0 Å achieved after screening several crystals with enhanced rigid body restraints applied to the structure and data beyond 1.0 Å resolution excluded from the refinement. An empirical absorption correction determined using SADABS[5] was applied to the data.

The asymmetric unit (Figure S1 (a)) consisted of half a BPPFTzTz ligand. The structure showed two-fold disorder of the fluorine substituents and a planar TzTz-phenyl backbone with lateral offsets of the outer pyridine rings of ~53°. The crystal packing shows alternating stacks of BPPFTzTz units when viewed along the *a*-axis (Figure S1 (b)). The BPPFTzTz ligands within the extended structure exhibited π-stacking such that the ligands in each stack were separated by an inter-planar distance of 3.7590(8) Å.

Crystallographic Tables

Table S1. Crystallographic data and refinement details for **ZnFTzTz**.

Parameter	ZnFTzTz
Empirical formula	$C_{38}H_{30}N_6O_6F_2S_3Zn$
Formula weight	866.23
Temperature / K	150.01(10)
Crystal system	orthorhombic
Space group	*Pccn*
a / Å	26.0566(2)
b / Å	18.5354(2)
c / Å	15.67380(10)
α / °	90
β / °	90
γ / °	90
Volume / Å^3	7569.97(11)
Z	8
ρ_{calc} / g cm^{-3}	1.520
μ / mm^{-1}	3.011
$F(000)$	3552
Crystal size / mm^3	0.216 × 0.167 × 0.063
Radiation	CuK$_\alpha$ (λ = 1.54184 Å)
2Θ range for data collection / °	5.852 to 147.982
Index ranges	$-29 \leq h \leq 32, -21 \leq k \leq 23, -19 \leq l \leq 19$
Reflections collected	53560
Independent reflections	7625 [R_{int} = 0.0418, R_{sigma} = 0.0233]
Data / restraints / parameters	7625 / 2 / 435
Goodness-of-fit on F^2	1.030
Final R indexes [I ≥ 2σ(I)]	R_1 = 0.0653, wR_2 = 0.2036
Final R indexes [all data]	R_1 = 0.0710, wR_2 = 0.2099
Largest diff. peak / hole / e Å^{-3}	0.78 / -1.34

* $R_1 = \Sigma||F_o| - |F_c||/\Sigma|F_o|$ for $F_o > 2\sigma(F_o)$; $wR_2 = (\Sigma w(F_o^2 - F_c^2)^2/\Sigma(wF_c^2)^2)^{1/2}$ all reflections $w=1/[\sigma^2(F_o^2) + (0.0896P)^2 + 13.3135P]$ where $P=(F_o^2 + 2F_c^2)/3$

Table S2. Crystallographic data and refinement details for BPPFTzTz.

Parameter	BPPFTzTz

Empirical formula	$C_{26}H_{14}N_4F_2S_2$
Formula weight	484.53
Temperature / K	100(2)
Crystal system	monoclinic
Space group	$P2_1/c$
***a* / Å**	24.130(5)
***b* / Å**	3.7590(8)
***c* / Å**	11.591(2)
α / °	90
β / °	103.34(3)
γ / °	90
Volume/ Å^3	1023.0(4)
Z	2
ρ_{calc} / g cm^{-3}	1.573
μ / mm^{-1}	0.304
***F*(000)**	496
Crystal size / mm^3	0.090 × 0.011 × 0.007
Radiation	Synchrotron (λ = 0.71073 Å)
2Θ range for data collection / °	1.734 to 41.628
Index ranges	$-24 \le h \le 24$, $-3 \le k \le 3$, $-11 \le l \le 11$
Reflections collected	6568
Independent reflections	1064 [R_{int} = 0.4916, R_{sigma} = 0.3932]
Data / restraints / parameters	1064 / 132 / 164
Goodness-of-fit on F^2	1.016
Final R indexes [I ≥ 2σ(I)]	R_1 = 0.1896, wR_2 = 0.4316
Final R indexes [all data]	R_1 = 0.2435, wR_2 = 0.4737
Largest diff. peak / hole / e Å^{-3}	0.39 / -0.36

* $R_1 = \Sigma||F_o| - |F_c||/\Sigma|F_o|$ for $F_o > 2\sigma(F_o)$; $wR_2 = (\Sigma w(F_o^2 - F_c^2)^2/\Sigma(wF_c^2)^2)^{1/2}$ all reflections $w=1/[\sigma^2(F_o^2) + (0.0896P)^2 + 13.3135P]$ where $P=(F_o^2 + 2F_c^2)/3$

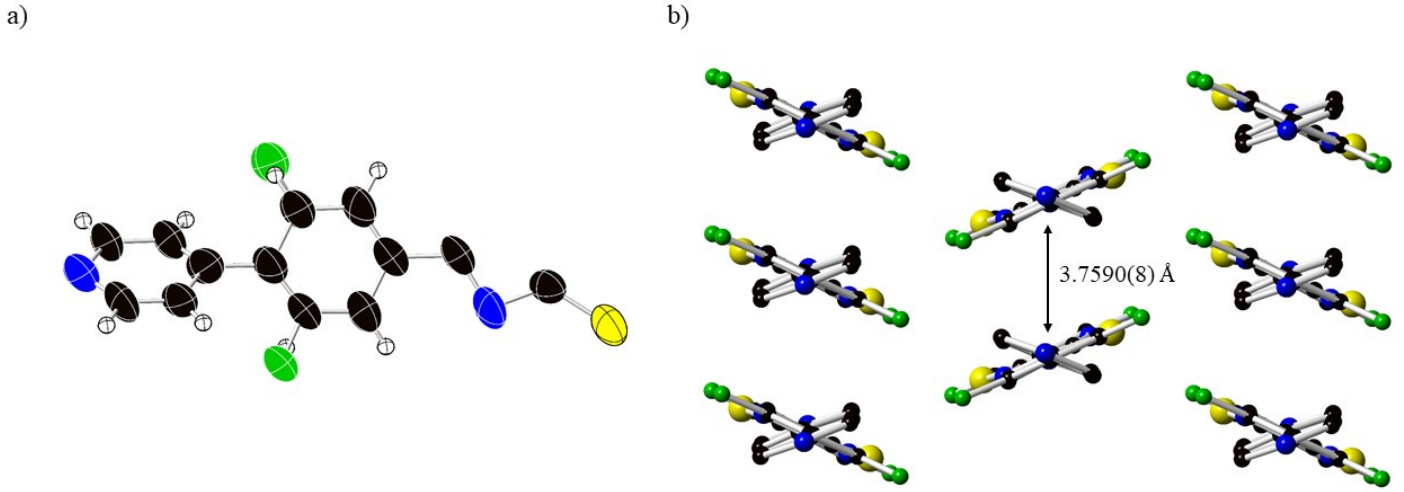

Figure S1. Crystal structure of the BPPFTzTz ligand showing a) the asymmetric unit and fluorine disorder components with thermal ellipsoids at 50% probability and b) packing of the crystal structure viewed down the *b*-axis showing the cofacial inter-planar distance of the BPPFTzTz ligands. Atom labelling: S = yellow, F = green, N = blue, C = grey and H = white. The hydrogen atoms in b) have been omitted for clarity.

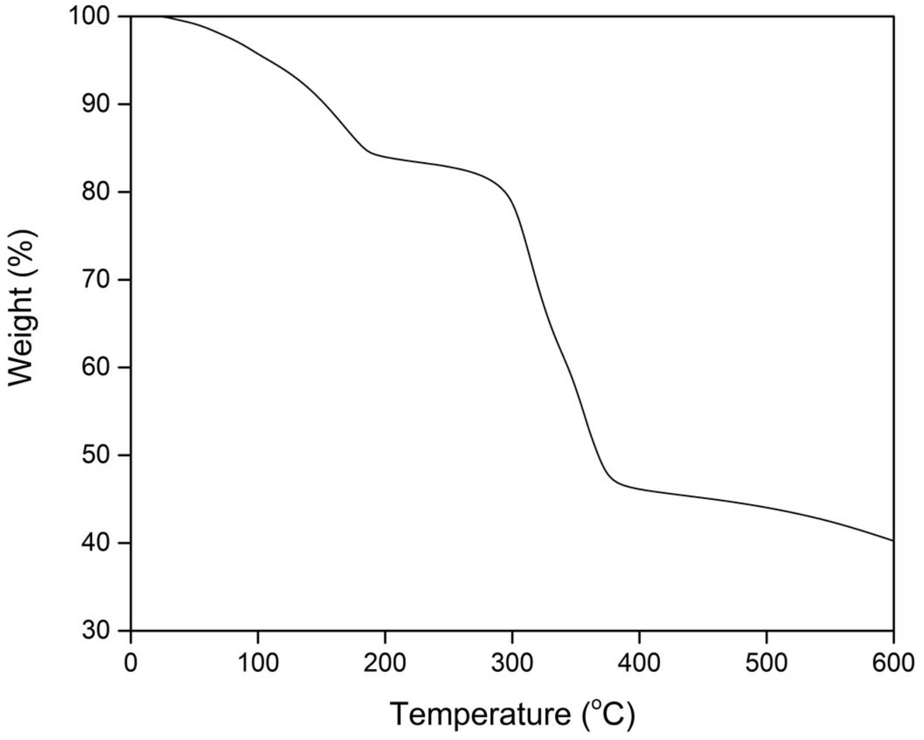

Figure S2. Thermal gravimetric analysis of **ZnFTzTz** from 25-600 °C at 2 °C min^{-1}.

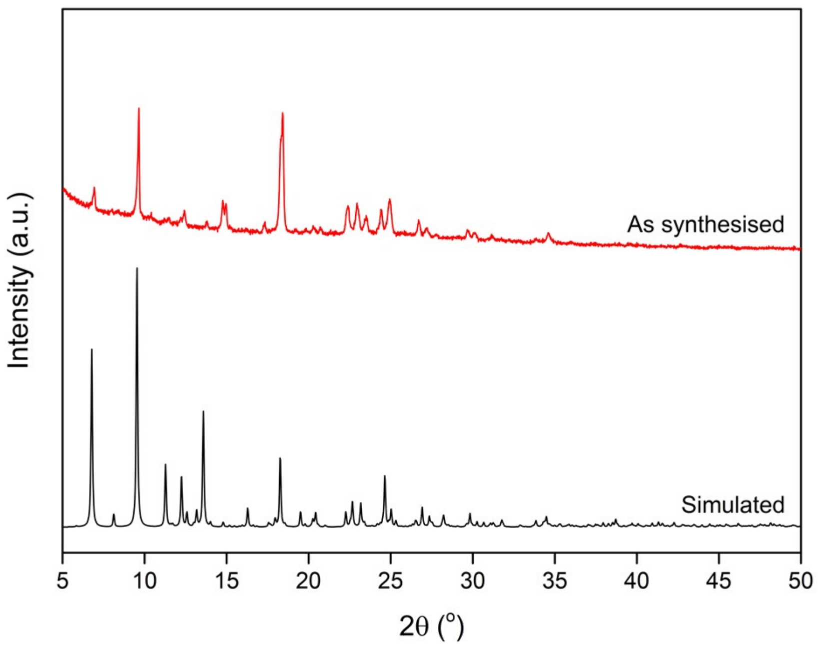

Figure S3. Room temperature powder X-ray diffraction pattern of bulk **ZnFTzTz** *vs*. the predicted pattern obtained from the single crystal structure at 150 K.

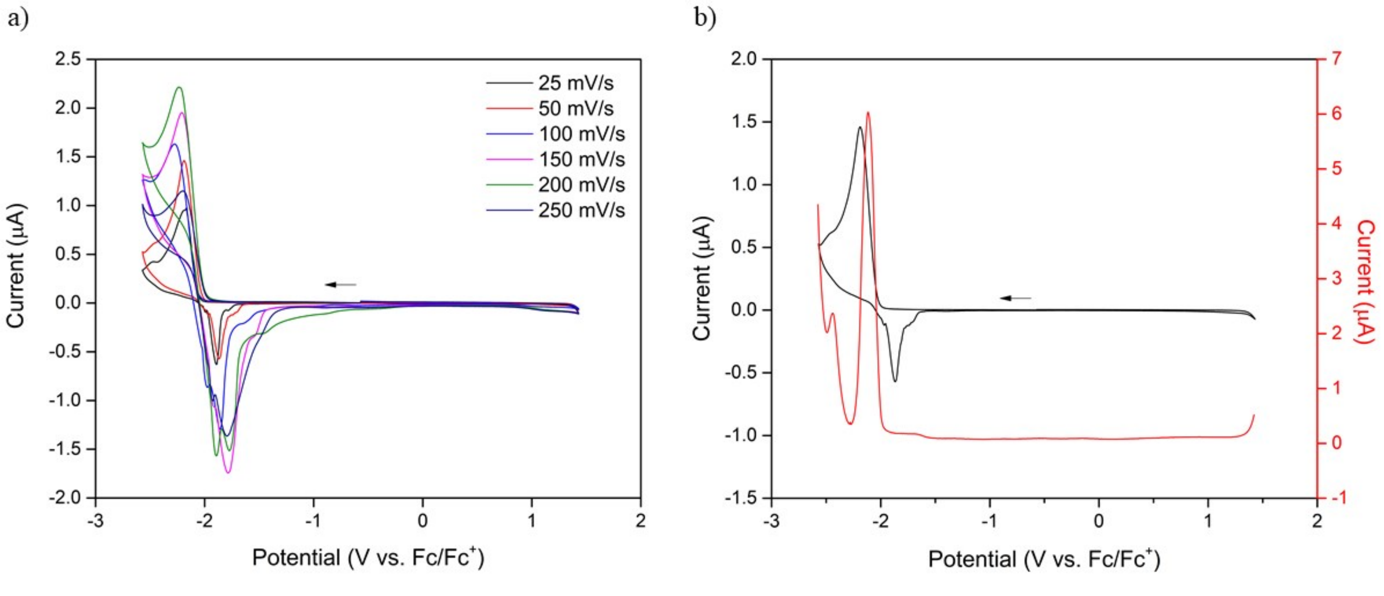

Figure S4. Solid-state electrochemistry of the BPPFTzTz ligand in 0.1 M $[(n\text{-}C_4H_9)_4N]PF_6$/MeCN supporting electrolyte showing a) cyclic voltammetry over a scan rate range of 25-250 mV/s and b) square wave voltammogram at an amplitude of 25 mV and a frequency of 15 Hz *vs*. the cyclic voltammogram at 50 mV/s. The arrows indicate the direction of the forward scan.

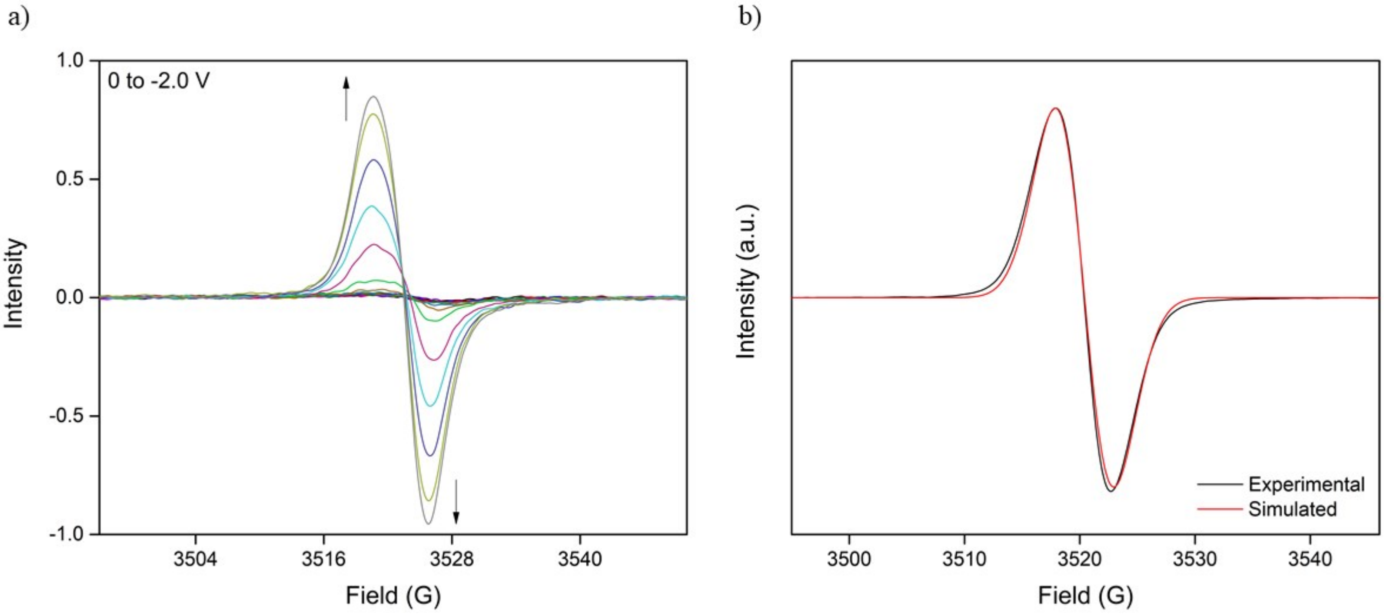

Figure S5. a) Solid-state X-band EPR spectroelectrochemistry of the BPPFTzTz ligand in 0.1 M [(n-C_4H_9)$_4$N]PF_6/MeCN electrolyte at applied potentials of 0 to −2.0 V where the arrows indicate the direction of the spectral evolution and b) Experimental *vs*. simulated spectra (using an isotropic model with $g_{iso} = 2.0073$ and an isotropic Gaussian linewidth of 4.2 mT) of the signal recorded under an applied potential of −2.0 V.

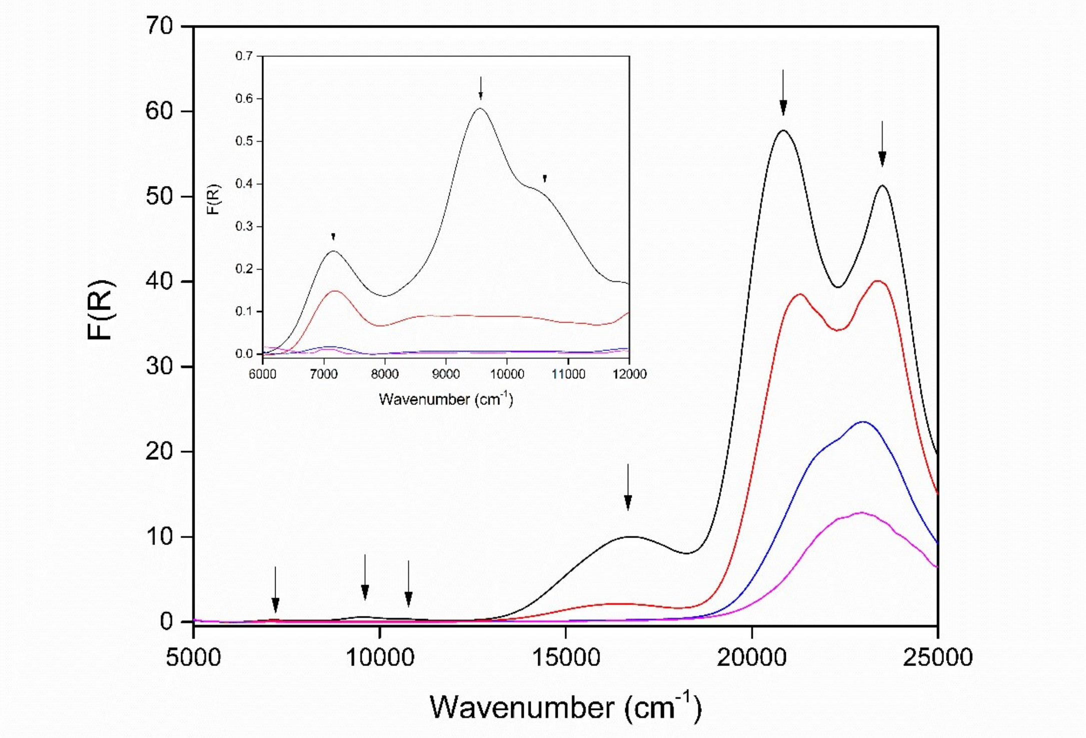

Figure S6. UV-Vis-NIR spectroelectrochemistry of **ZnFTzTz** in 0.1 M [(n-C_4H_9)$_4$N]PF_6/MeCN supporting electrolyte showing potential changes from -2.45 to 0 V where the arrows indicate the direction of the spectral progression. Insert: spectral changes in the NIR region upon returning the potential to 0 V showing the loss of the IVCT bands.

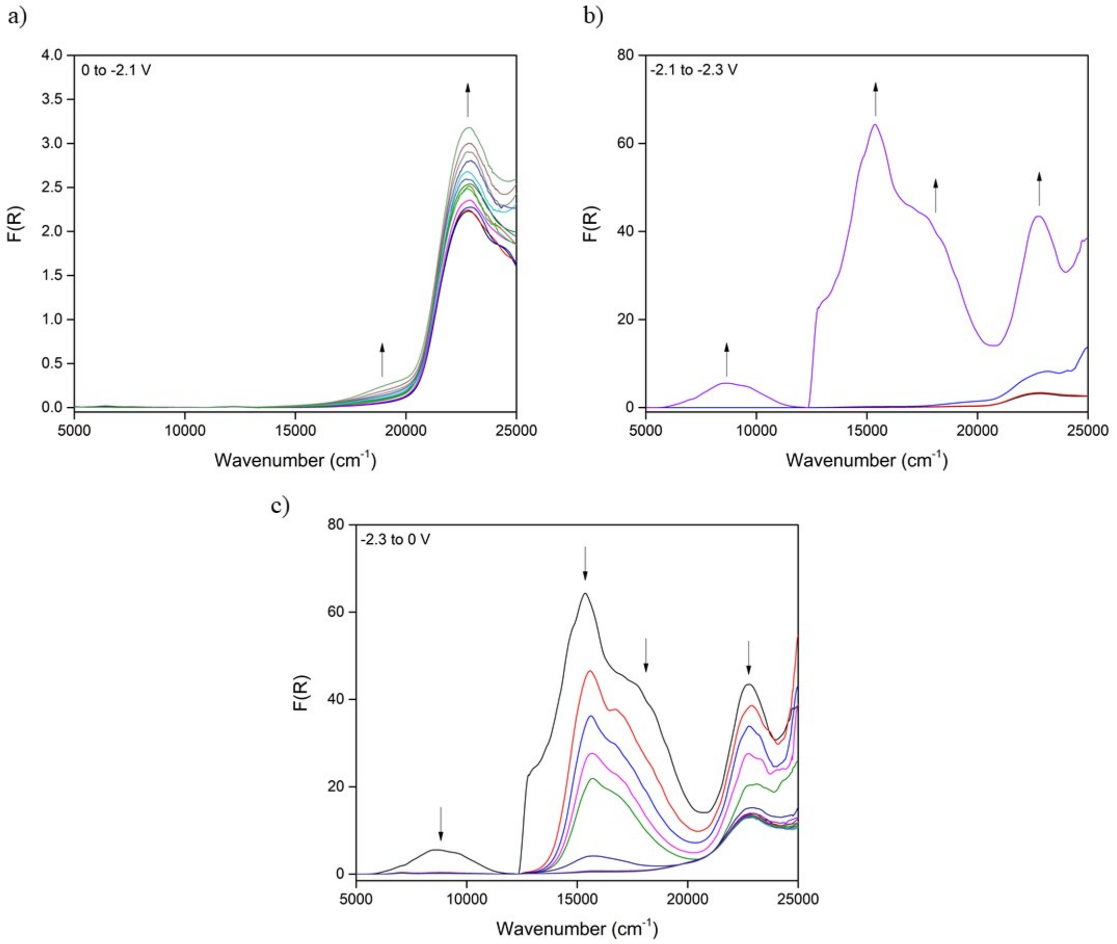

Figure S7. Solid-state UV-Vis-NIR spectroelectrochemistry of BPPFTzTz in 0.1 M $[(n\text{-}C_4H_9)_4N]PF_6$/MeCN electrolyte showing potential changes from a) 0 to −2.1 V, b) −2.1 to −2.3 V and −2.3 to 0 V where the arrows indicate the direction of the spectral progression. The step at 12500 cm^{-1} is due to the detector change.

Table S3. Amount of LiNP reductant added to the **ZnFTzTz** framework and amount of intercalated Li as determined by ICP-MS.

LiNP Reductant Added (Eq.)	Actual Amount of LiNP Reductant (Eq.)	Li (mol)	Zn (mol)	Ratio (Li:Zn)
0.5	0.39	0.46	1.19	1 : 2.56
1.0	0.65	0.56	0.87	1 : 1.55
2.0	1.25	3.73	2.99	1 : 0.80
3.0	1.67	2.19	1.31	1 : 0.60
4.0	2.17	2.39	1.01	1 : 0.46
5.0	3.37	3246.4	961.6	1 : 0.30

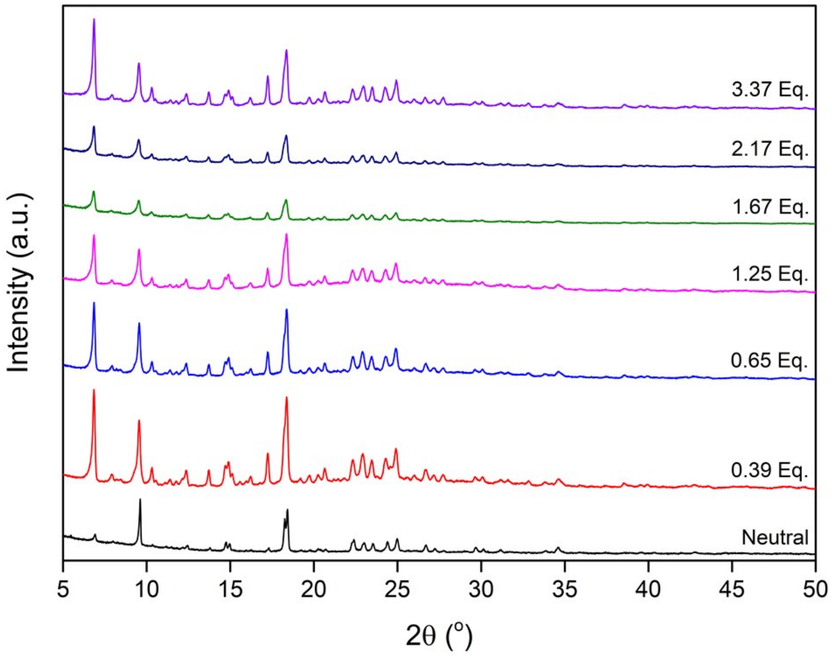

Figure S8. PXRD patterns of the chemically reduced **ZnFTzTz** material upon reduction with the indicated equivalent of LiNP.

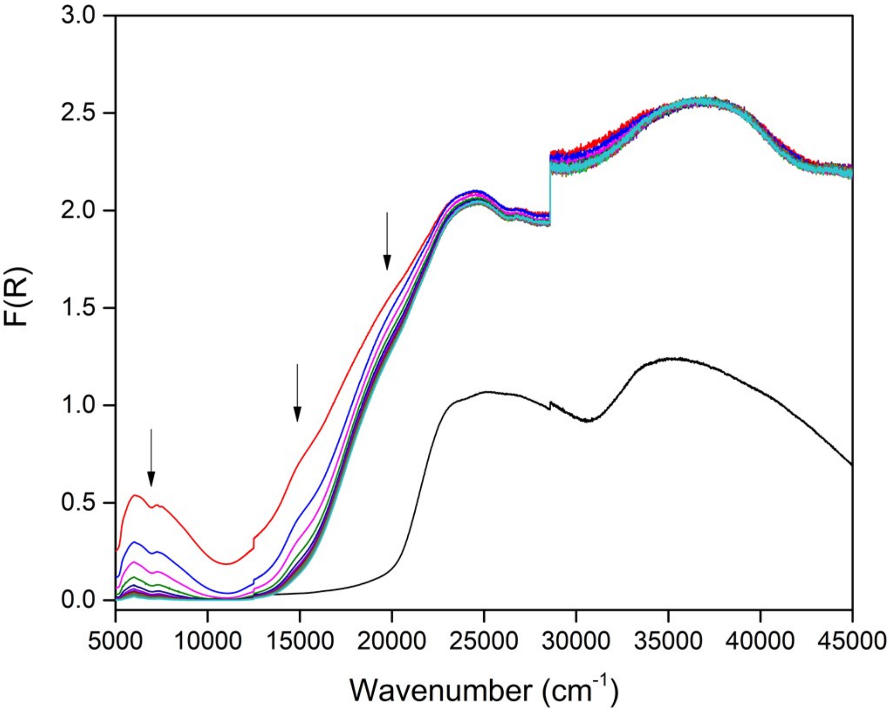

Figure S9. Solid-state UV-Vis-NIR spectra of **ZnFTzTz** upon auto-oxidation of a reduced sample reacted with 1.67 Eq. of LiNP (red) in air. The black curve corresponds to the spectrum of the neutral, as synthesised framework. The arrows indicate the direction of the spectral progression and the steps at 12500 and 28600 cm^{-1} are due to detector changes.

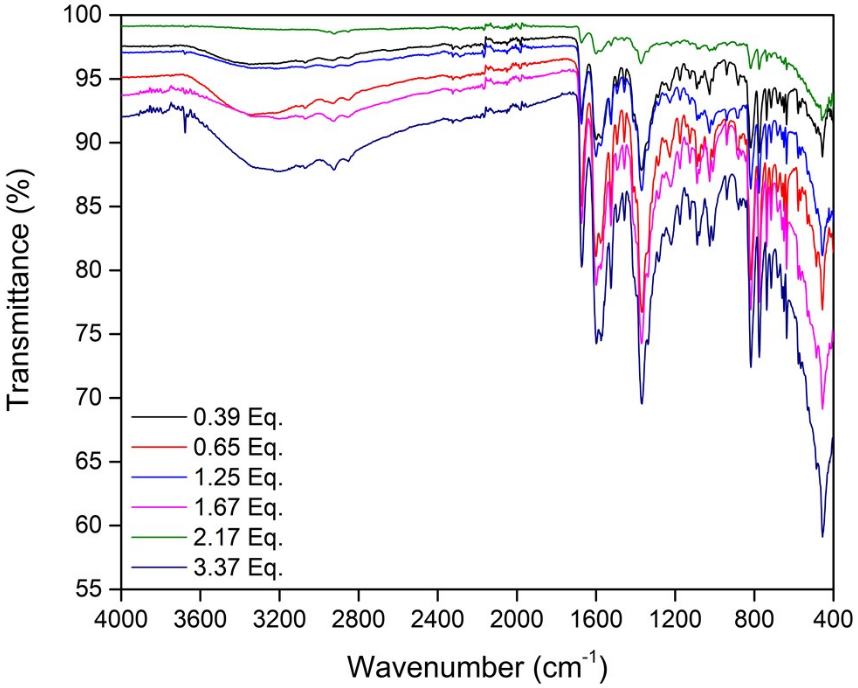

Figure S10. IR spectra of the **ZnFTzTz** material post-chemical reduction with 0.1 M LiNP solution.

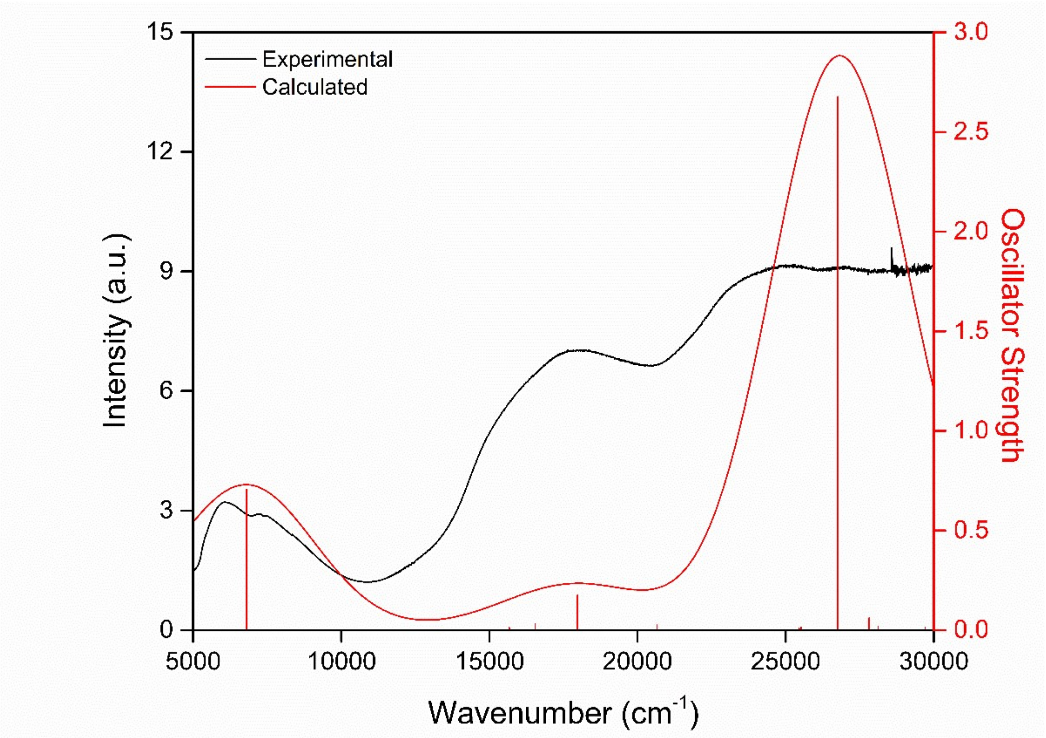

Figure S11. Experimental *vs.* simulated UV-Vis-NIR spectra of reduced **ZnFTzTz** at the BMK/6-311G(d) level of theory in DMF solvent where the vertical bars correspond to the calculated excited states.

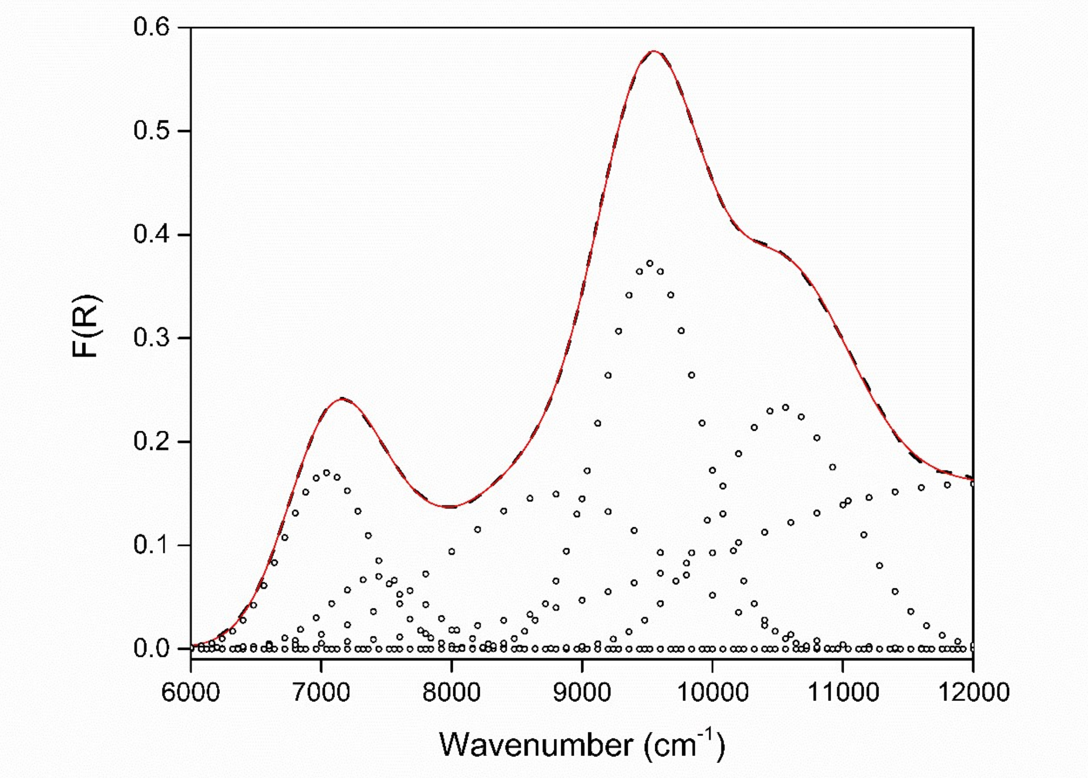

Figure S12. Experimental (black dashes) vs. deconvoluted curvefit (red) of the solid-state UV-Vis-NIR spectrum of the mixed-valence form of **ZnFTzTz** with underlying Gaussian components (dotted lines) of the deconvolution. Gaussian deconvolution was performed using the GRAMS suite of software.

Equations Used to Derive Charge Transfer Parameters

Theoretical bandwidth:

$$\Delta v_{1/2}{}^{o} = [2310(v_{max})]^{1/2} \qquad \text{(Eqn. 1)}$$

where v_{max} is the position of the relevant band (in cm^{-1}).[6,7] Note that the "theoretical" bandwidth here is a semi-empirical quantity derived from the position of the band maximum v_{max}.

Tunnelling matrix element:

$$T_{da} = [(4.2 \times 10^{-4}) \times \varepsilon_{max} \Delta v_{1/2} E_{op}]^{1/2}/d \qquad \text{(Eqn. 2)}$$

where E_{op} is the energy of the IVCT band (v_{max} in cm^{-1}), ε_{max} is the extinction coefficient (in $\mathrm{M}^{-1}\ \mathrm{cm}^{-1}$) and d is the charge transfer distance (equivalent to r_{ab} from Eqn. 7, in Å). All quantities in cm^{-1} are divided by 10^3 as per this equation's definition by Hush.[7,8]

Frequency factor:

$$v_{et} = [4\pi^2 T_{da}{}^2 / h](\pi / k_B T \lambda)^{1/2} \qquad \text{(Eqn. 3)}$$

where h is Planck's constant (4.136×10^{-15} eV s), k_B is Boltzmann's constant (8.617×10^{-5} eV K^{-1}), T is the temperature (300 K) and λ (i.e. v_{max}) is the energy of the IVCT band (in eV).[9]

Mobility:

$$k = v_{et}\, e^{\frac{-\chi}{4RT}} \qquad \text{(Eqn. 4)}$$

where χ is the molar energy of electron transfer obtained by multiplying λ (i.e. v_{max}) with Avogadro's constant and R is the ideal gas constant ($8.314 \times 6.242 \times 10^{18}$ eV K^{-1} mol^{-1}).[9]

Quantification of the IVCT Bands *via* Single Crystal UV-Vis Absorption Spectroscopy

The IVCT bands of the mixed-valence **ZnFTzTz** material were quantified using a recently reported methodology.[10] A single crystal UV-Vis experiment, using the method of Krausz,[11] was performed on a single crystal of the neutral **ZnFTzTz** material to obtain the solid-state absorption spectrum (Figure S13) from which a solid-sate molar extinction coefficient could be obtained. Care was taken to choose a well-defined single crystal, i.e. with a regular morphology and no cracks or satellite crystallites, to prevent undesirable absorption or scattering effects.

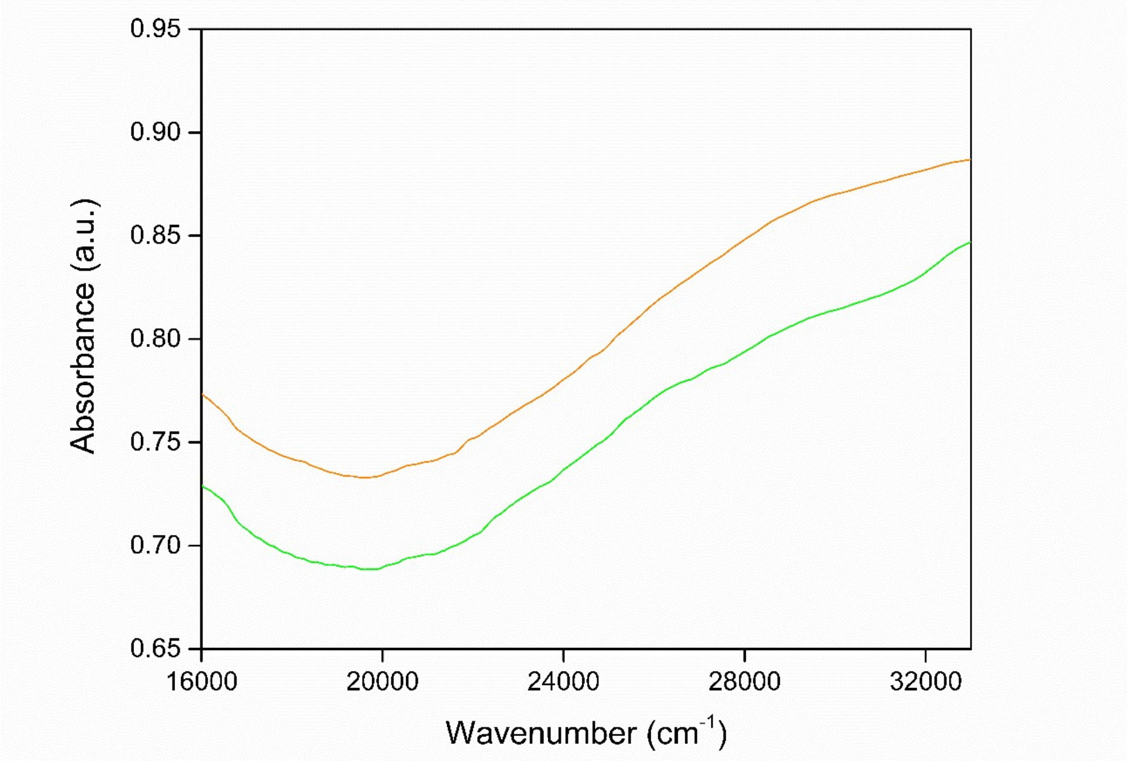

Figure S13. Single crystal UV-Vis spectra of **ZnFTzTz** showing absorbance in both parallel (orange) and perpendicular (green) polarisation modes. The two modes are relative to the plane of polarisation of the incident light.

The absorption spectrum was analysed using the Beer-Lambert law.

$$A = \varepsilon c l \qquad \text{(Eqn. 5)}$$

The value of the absorbance pathlength (l) was obtained from measurement of the physical dimensions of the crystal using the optical viewer of a single crystal X-ray diffractometer.

The solid-state molar extinction coefficient was derived from the number concentration definition:

$$n = \frac{n}{V} = \frac{N}{N_A V} \qquad \text{(Eqn. 6)}$$

where N is the number of chromophores per crystallographic unit cell, N_A is Avogadro's constant and V is the unit cell volume (in L).

Within the **ZnFTzTz** structure, the number of BPPFTzTz chromophores in the asymmetric unit is one, hence N is equal to the Z number of the structure to give 8 BPPFTzTz chromophores per unit cell. Evaluating Eqn. 6 with these parameters yielded a solid-state molar concentration value of 1.75 M for the **ZnFTzTz** framework. The solid-state molar extinction coefficient was then derived from the Beer-Lambert law (Table S4).

Table S4. Spectral parameters derived from single crystal UV-Vis spectroscopy of **ZnFTzTz**.

Parameter	**ZnFTzTz**
N	8
Concentration (M)	1.75
Pathlength (cm)	0.0026
Absorbance Maximum (a.u.)	0.88
Molar Extinction Coefficient (M^{-1} cm^{-1})	191.2

Given that the molar extinction coefficients had been calculated for the neutral MOFs, the extinction coefficient of the mixed-valence species could be calculated by multiplying this by the ratio of the neutral and NIR band F(R) values. An assumption to note here is that the extinction coefficient values are linear across the entire wavelength range. From these, the electronic coupling constants (H_{ab}) of the NIR IVCT bands of both materials could be calculated by applying the Marcus-Hush equation (Eqn. 7).[6,7]

$$H_{ab} = [0.0205 \times (\nu_{max}\varepsilon\Delta\nu_{1/2})^{1/2}] / \mathrm{r}_{ab} \qquad \text{(Eqn. 7)}$$

where ν_{max} is the energy of the IVCT band and $\Delta\nu_{1/2}$ is the bandwidth obtained from deconvolution, ε is the extinction coefficient of the IVCT band and r_{ab} is the crystallographically determined distance between the cofacial BPPFTzTz ligand pair (in Å). Evaluating this equation with the derived parameters obtained from deconvolution of the diffuse reflectance spectra yielded the H_{ab} of the mixed-valence **ZnFTzTz** MOF (Table S5).

Table S5. Spectral data of the deconvoluted diffuse reflectance spectrum of the reduced **ZnFTzTz** material.

ν_{max} (cm^{-1})	F(R)$_{\max}$ (a.u.)	$\Delta\nu_{1/2}$ (cm^{-1})	$\Delta\nu_{1/2}{}^{o}$ (cm^{-1})	ε (M^{-1} cm^{-1})	H_{ab} (cm^{-1})
7043	0.17	795	4034	36.3	78
7436	0.07	864	4145	15.3	54
8795	0.149	1949	4507	32.5	128
9520	0.372	910	4689	80.3	143
10534	0.234	1203	4933	51.6	139
12000	0.159	4529	5265		

where $\Delta\nu_{1/2}{}^{o} = [2310(\nu_{\max})]^{1/2}$ at 298 K.[6-8,12]

References

1. Aragao, D.; Aishima, J.; Cherukuvada, H.; Clarken, R.; Clift, M.; Cowieson, N. P.; Ericsson, D. J.; Gee, C. L.; Macedo, S.; Mudie, N.; Panjikar, S.; Price, J. R.; Riboldi-Tunnicliffe, A.; Rostan, R.; Williamson, R.; Caradoc-Davies, T. T. *J. Synchrotron Rad.* **2018**, *25*, 885.
2. Sheldrick, G. *Acta Cryst.* **2015**, *A71*, 3.
3. Sheldrick, G. *Acta Cryst.* **2015**, *C71*, 3.
4. Hubschle, C. B.; Sheldrick, G. M.; Dittrich, B. *J. App. Cryst.* **2011**, *44*, 1281.
5. Bruker (2001). *SADABS*. Bruker AXS Inc., Madison, Wisconsin, USA.
6. Allen, G. C.; Hush, N. S. *Prog. Inorg. Chem.* **1967**, *8*, 357.
7. Hush, N. S. *Prog. Inorg. Chem.* **1967**, *8*, 391.
8. Hush, N. S. *Electrochim. Acta* **1968**, *13*, 1005.
9. Meyer, T. J. *Chem. Phys. Lett.* **1979**, *64*, 417.
10. Doheny, P. W.; Clegg, J. K.; Tuna, F.; Collison, D.; Kepert, C. J.; D'Alessandro, D. M. *Chem. Sci.* **2020**, *11*, 5213.
11. Krausz, E. *Aust. J. Chem.* **1993**, *46*, 1041.
12. D'Alessandro, D. M.; Keene, F. R. *Chem. Soc. Rev.* **2006**, *35*, 424.